Dynamic Range Improvements for Beacon Receivers Using Noise Power Measurements

Étienne Suquet, Laurent Castanet, Laurent Féral, Hugo Bourgoin, Xavier Boulanger

Dynamic Range Improvements for Beacon Receivers Using Noise Power Measurements

Étienne Suquet, Laurent Castanet, Laurent Féral, Hugo Bourgoin and Xavier Boulanger

***Abstract*—Satellite beacon receivers are metrology instruments measuring beacon power in order to determine excess tropospheric attenuation. In presence of thermal noise, beacon power measurements are biased and should be corrected a posteriori using unbiased (or with minimum bias) estimators to remove or at least to reduce the noise contribution. When satellite beacon receivers are able to measure the noise power level in a frequency band adjacent to the beacon frequency band, it is shown that this additional information can be used opportunely to reduce the estimation bias. In this context, three estimators are discussed, one of which is an originality introduced to take into account the particular processing of beacon measurements. The performances of these estimators are assessed using synthetic time series simulating beacon measurements. For the new estimator, the results show a dynamic range improvement of about 12 dB, using typical beacon receiver characteristics. When considering long-term statistics of attenuation, the improvement is even larger. The estimators are applied to experimental beacon receiver data collected in Ka and Q bands in Toulouse (France). The results confirm the potentiality of the approach to improve significantly the dynamic range of beacon measurements.**

***Index Terms*—propagation, signal processing, power estimation, tropospheric attenuation, beacon measurements**

I. Introduction

SATELLITE SYSTEMS are transitioning to high frequency bands (Ka-band and above), benefiting from wider bandwidth in order to provide higher data rates. At these frequencies, tropospheric attenuation (that can amount to several tens of decibels, mainly due to rain) severely affects system performances and must be quantified. Beacon receivers are metrology instruments used to derive experimental time series of rain attenuation with good accuracy and high dynamic range [1], using post-processing techniques to remove both hardware issues (antenna mispointing, RF chain drifts, etc.), free space loss and clear sky atmospheric conditions [2].

Beacon data have proven to be useful not only to produce statistics of rain attenuation to determine link budget margins in the design of satcom systems, but also to quantify the attenuation in real time to optimise fade mitigation techniques control loops (such as uplink power control) [3].

The design of beacon receivers has been extensively studied in the literature (e.g. [4], [5], [6], [7], [8]). In particular, one of the figures of performance of a beacon receiver is its dynamic range, which characterises the range of attenuation it can accurately measure. The dynamic range of a beacon receiver depends on the quality of its components (such as its noise figure, receiving chain linearity, etc.), on the signal processing techniques used [9], but also on the level of thermal noise. Thermal noise, intrinsically of random nature, artificially enhances the "true" power at the input of the receiver while preventing any exploitable measurements below the noise floor. Therefore, in presence of thermal noise, beacon receivers do not measure only the power coming from the beacon but rather a noisy power that should be corrected a posteriori, using unbiased (or with minimum bias) estimators to remove or at least to reduce the noise contribution.

This is the object of the present paper, which proposes a methodology to improve the dynamic range of a beacon receiver thanks to the concurrent measurement of the noise power in a frequency band adjacent to the beacon frequency band.

The paper is organised as follows. In Section II, the generic architecture of a beacon receiver is presented, along with the hypotheses on the signal and the receiver used throughout the paper. Section III defines the parameters of interest and discusses dynamic range definitions. Section IV is devoted to the mathematical derivations of estimators of the power of the beacon signal. The performances of these estimators are then compared in Section V using numerical simulations of a beacon receiver fed with synthetic power time series. In Section VI, the impact of the measurement bandwidth on the dynamic range is discussed. Finally, section VII discusses the applicability of the newly derived estimator to actual experimental beacon data measured at Ka and Q bands.

II. Beacon Receiver Model

Being metrology instruments, beacon receiver design is quite specific. Nevertheless, from a signal processing point of view, their architecture can be reduced to a few elementary functions. Typically, beacon receivers are composed of two parts. The analogic part fulfils the functions of amplification of the signal, mixing (for the purpose of shifting the signal to a lower frequency), filtering and digitization, as depicted in Fig. 1. The digital part, shown in Fig. 2, measures the power of the signal in a narrow band, the beacon frequency band (bandwidth B_S), centred around the beacon carrier frequency f_b. Importantly, some beacon receivers (e.g. [8]) also measure the noise power N in a wider frequency band, adjacent to the beacon frequency band in order to evaluate the noise power

Étienne Suquet, Laurent Castanet and Hugo Bourgoin are with the ONERA/DEMR, Université de Toulouse, Toulouse F-31055, France (e-mails: etienne.suquet@onera.fr, laurent.castanet@onera.fr, hugo.bourgoin@onera.fr).

Laurent Féral is with the Laboratoire d'Aérologie (LAERO), Université de Toulouse, CNRS, UT3, IRD, Toulouse, France (e-mail: laurent.feral@aero.obs-mip.fr).

Xavier Boulanger is with the Centre National d'Études Spatiales (CNES), DTN/TPI/TCP, Toulouse, France (e-mail: xavier.boulanger@cnes.fr).

spectral density N_0, as illustrated in Fig. 3. One possible application is to use the receiver as a radiometer (e.g. [4], [10]). In this paper, this frequency band containing noise will be referred to as the 'adjacent frequency band', with a bandwidth B_N. Typically, B_S amounts for a few tens of hertz, and B_N for several kHz.

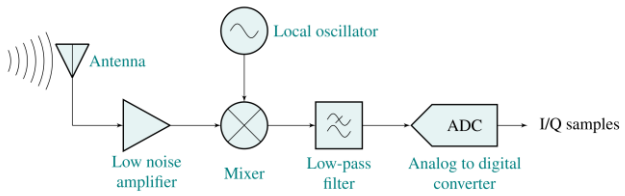

Fig. 1. Simplified block diagram of the analogic part of a generic beacon receiver.

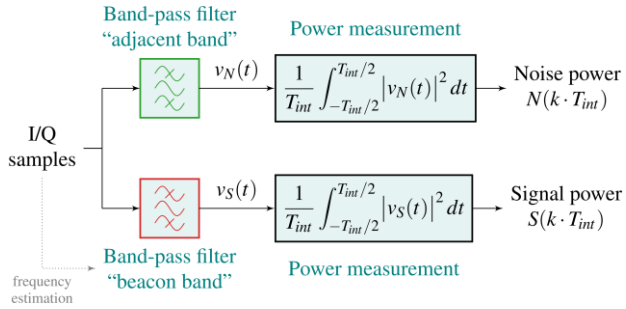

Fig. 2. Block diagram of the digital part of a generic beacon receiver and its outputs.

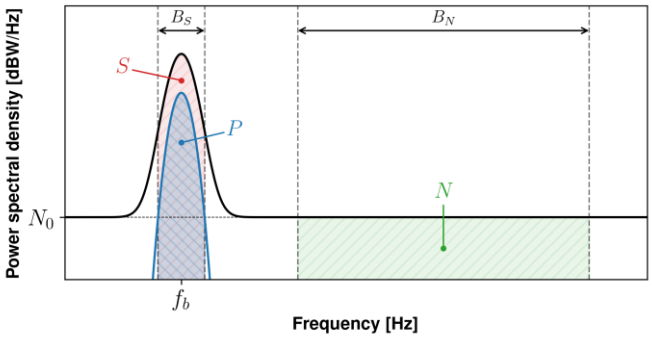

Fig. 3. Illustration of the power spectral density of a beacon receiver, as well as the power measurements (P, S and N) over the beacon and adjacent frequency bands, which bandwidth are respectively B_S and B_N. f_b is the beacon frequency. P is the noiseless power in the beacon frequency band without the effect of thermal noise. S is the power actually measured in the same frequency band in presence of thermal noise. N is the noise power in the adjacent frequency band solely affected by thermal noise.

The digital part of the beacon receiver (Fig. 2) can be implemented in various ways. Filtering and power measurements can be performed either in the time domain or in the Fourier frequency domain, with equivalent results from Parseval's theorem. Sometimes, a non-rectangular integration window is used in the time domain, such as in [4]. Using particular windows can reduce the spectral leakage with respect to rectangular windows, but will reduce the signal-to-noise ratio [11]. The equivalent noise bandwidth of a rectangular window being the lowest possible, a rectangular window is used in this paper, with the advantage of simplifying analytic formulations. Further considerations about spectral leakage are discussed in Section VI. Also, some authors use overlapping power estimates, such as in [4]. While for a fixed sampling frequency, such estimates are more precise than non-overlapping ones (being integrated over longer durations), they introduce a correlation between the samples, which effectively leads to a reduction of the sampling frequency. As a consequence, in the following sections, power measurements are computed using non-overlapping rectangular windows.

In order to derive the estimators, it is assumed that apart from the thermal noise generated by the sky and the beacon receiver itself, all the components are ideal: amplifiers are assumed to be perfectly linear, the local oscillator does not generate phase noise, the filters have a flat frequency response, the quantization noise from the Analog to Digital Converter (ADC) is negligible, and the band-pass filters have a perfect rectangular frequency response. Some of these hypotheses will be reconsidered in Section VII. Besides, the thermal noise is modelled as an Additive, White Gaussian Noise (AWGN), which is a common assumption [12].

III. Parameters and Dynamic Range Definitions

A. Definition of the main data processing parameters

Beacon receivers retrieve experimental time series of attenuation $A(t)$ from power measurements in the frequency band of the satellite beacon, coupled with post-processing techniques [13], summarized hereinafter. A first step is to synchronize all data to a common reference time. Afterwards, doubtful and erroneous data are flagged. Then, the raw time series of power $S(t)$ are converted to decibels ($S_{dBW}(t)$) and low-pass filtered ($S_{dBW}^{filt}(t)$) with a cut-off frequency f_c (usually 0.025 Hz in temperate climates [14]) in order to remove fast fluctuations of the signals, mainly caused by tropospheric scintillation. It has to be stressed that the power is low-pass filtered in decibel-watts (dBW), rather than watts, as it is admitted that the tropospheric scintillation has a centred, normal distribution when expressed in decibels (at least for weak scintillations under conditions of stationarity [15]). Finally, the experimenter defines a reference power level $P_{dBW}^{ref}(t)$, from which attenuation $A_{dB}(t)$ is defined as

$$A_{dB}(t) \stackrel{\text{def}}{=} P_{dBW}^{ref}(t) - P_{dBW}^{filt}(t), \qquad (1)$$

where $P_{dBW}^{filt}(t)$ is the power from low frequency components (below the frequency f_c) mainly associated to tropospheric attenuating effects, that would be measured by a perfect beacon receiver (in particular, with no influence from any sort of noise). Because actual measurements are always affected by noise, $P_{dBW}^{filt}(t)$ is unknown, and once $P_{dBW}^{ref}(t)$ is set, determining the attenuation consists in estimating $P_{dBW}^{filt}(t)$ from the measurement $S_{dBW}^{filt}(t)$, which is the subject of this paper.

Whether $A_{dB}(t)$ refers to rain attenuation, an aggregation of rain and clouds attenuation, or total tropospheric attenuation depends on the definition of $P_{dBW}^{ref}(t)$, which is decided by the experimenter (sometimes, $P_{dBW}^{ref}(t)$ is set using additional instruments, such as radiometers [13], or other methods [16]). The estimation of $P_{dBW}^{filt}(t)$ is therefore independent of which tropospheric attenuating effects are considered.

The dynamic range of a beacon receiver is affected by thermal noise, whose power in the frequency band of the beacon (B_S) is noted $\sigma_S^2(t)$. Thermal noise artificially enhances the 'true' power $P(t)$ – and so $P_{dBW}^{filt}(t)$ – at the

receiver while preventing any exploitable measurements below the noise floor. Therefore, in presence of thermal noise, beacon receivers do not measure $P(t)$ but rather a noisy power $S(t)$ (see Fig. 3) that should be corrected for noise a posteriori, using unbiased (or with minimum bias) estimators $\hat{P}$.

Three estimators $\widehat{P_{dBW}^{filt}}^{(i)}$, $i \in 1,2,3$ are considered. They all infer estimates $\widehat{A_{dB}}$ of the attenuation from beacon measurements S_{dBW}^{filt}:

$$\widehat{A_{dB}}(t) \stackrel{\text{def}}{=} P_{dBW}^{ref}(t) - \widehat{P_{dBW}^{filt}}^{(i)}(t). \tag{2}$$

The first estimator, $\widehat{P_{dBW}^{filt}}^{(1)}$, that is named the 'customary' estimator in this paper, consists in directly using the filtered beacon power measurements $\widehat{P_{dBW}^{filt}}^{(1)}(t) = S_{dBW}^{filt}(t)$, as it is customary when noise power measurements are not available. The second estimator, $\widehat{P_{dBW}^{filt}}^{(2)}$, proposed in [5], uses the additional measurement of the noise power density in the frequency band B_N adjacent to the one of the beacon. This estimator considers that the power is processed in its natural unit (i.e. in watts), hence it is referred to as the 'natural' estimator. Because it is established that the beacon measurements should be processed in decibel-watts (in particular the low-pass filter with a cut-off frequency f_c mentioned previously), and the logarithm is a non-linear transformation, the natural estimator is actually biased. Nevertheless, it will be shown in this paper that the bias of the natural estimator is still lower than the bias of the customary estimator. Finally, the originality of this paper lays in the formulation of a third estimator $\widehat{P_{dBW}^{filt}}^{(3)}$, taking into account the bias introduced by the logarithm in the data processing. It is therefore named the logarithmic estimator.

B. Dynamic Range Definition

In electrical engineering, the dynamic range R_D is generally defined as the ratio (or the difference in decibels) between the highest and lowest values an instrument can measure with acceptable levels of distortion [17]. Nevertheless, what constitutes an acceptable level of distortion can be specified in different ways [18]: deviations from linearity (e.g. definitions using the 1-dB compression point), distance from noise floor (e.g. by specifying a minimum signal-to-noise ratio), etc. In the particular case of beacon receivers, the quantity of interest is the attenuation A_{dB}, so the dynamic range R_D is the difference

$$R_D \stackrel{\text{def}}{=} A_{dB}^{M} - A_{dB}^{m}, \tag{3}$$

between the highest attenuation A_{dB}^{M} and the lowest A_{dB}^{m} attenuation the instrument can measure without distortion. A properly designed beacon receiver should not distort the measurements in clear sky conditions, so that A_{dB}^{m} equals 0 dB (attenuation cannot be negative by definition). On the other hand, the definition of the highest measurable attenuation A_{dB}^{M} is not straightforward. It could be defined, for instance, as the mean attenuation measured by the beacon receiver when the signal is absent (noise floor), or as the mean attenuation measured for a particular signal-to-noise ratio. Depending on which definition is used, the dynamic range R_D can take a rather wide extent of values.

In propagation studies, the value of the dynamic range R_D is often given in order to characterize the performance of the beacon receiver. Nevertheless, its exact definition is rarely provided. One exception is [5] where the authors relate R_D to the signal-to-noise ratio, as described hereafter. Let $P(t)$ be the (deterministic) power level, in watts, at the output of a noiseless beacon receiver, and $S(t)$ the (random) power level, in watts, actually measured at the output of the receiver in presence of (random) thermal noise. Then the noisy beacon power S is a first estimator $\hat{P}^{(1)}$ of the ideal, noiseless, signal P. If, as commonly assumed, the thermal noise and the noiseless power P are independent, then the expected value $\mathbb{E}[S]$ (in watts) of the noisy beacon power S is the sum of P (in watts) and the noise power ${\sigma_S}^2$ (in watts) in the frequency band of the beacon (B_S):

$$\mathbb{E}[S] = \sigma_S^2 + P, \tag{4}$$

where $\mathbb{E}[\cdot]$ is the expectation operator. In presence of noise, σ_S^2 is strictly positive. Therefore, from (4), $\mathbb{E}[S]$ is greater than P. It follows that $\hat{P}^{(1)} \stackrel{\text{def}}{=} S$ is a (positively) biased estimator of P. In [5], a first definition of the 'measurement bias' $\Delta^{(1)}$ of the estimator S is proposed:

$$\begin{aligned} \Delta^{(1)} &\stackrel{\text{def}}{=} 10\log_{10}\left(\mathbb{E}\left[\frac{S}{P}\right]\right) \\ &= 10\log_{10}\left(\frac{\mathbb{E}[S]}{P}\right), \end{aligned} \tag{5}$$

with S and P in watts. Defining $SNR \stackrel{\text{def}}{=} P/\sigma_S^2$ as the signal-to-noise ratio measured in the beacon frequency band, (4) in (5) leads to:

$$\Delta^{(1)} = 10\log_{10}\left(1 + \frac{1}{SNR}\right). \tag{6}$$

A first definition of the dynamic range $R_D^{(1)}$ of a beacon receiver, inherited from [5], emerges:

$$R_D^{(1)} \stackrel{\text{def}}{=} \max\left\{ \widehat{A_{dB}}(t) \right\} \Big| \, \Delta^{(1)} \leq \Delta_{max}^{(1)} \tag{7}$$

where $\Delta_{max}^{(1)}$, in dB, is the maximum acceptable bias above which the signal is assumed too noisy to be usable in practice (i.e. it exceeds the dynamic range), and the vertical bar should be read *'such that'*. $R_D^{(1)}$ can be viewed as the maximum attenuation value that can be estimated with a bias smaller than $\Delta_{max}^{(1)}$. Fig. 4 illustrates the situation on a log scale (i.e. in dBW), considering the customary estimator. The measured beacon signal $S(t)$ remains in its dynamic range if the difference between its expected value $\mathbb{E}[S]$ and the noiseless signal P is smaller than $\Delta_{max}^{(1)}$ (right part of Fig. 4). On the contrary, when $\mathbb{E}[S]$ departs from P (left part of Fig. 4), the measurement bias $\Delta^{(1)}$ exceeds $\Delta_{max}^{(1)}$, so that the beacon signal S is outside its dynamic range and cannot be considered accurate. For instance, [5] considered that $\Delta_{max}^{(1)}$ is equal to 0.4 dB, leading to a minimum signal-to-noise ratio of approximately 10 dB according to (6). Thus, for beacon data users, (6) provides valuable information, that is the typical error originating from thermal noise when reaching the limits of the receiver dynamic range.

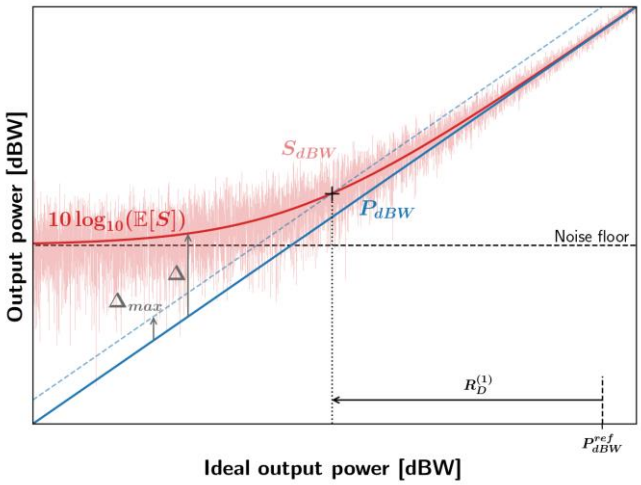

Fig. 4. Illustration of the dynamic range definition $R_D^{(1)}$ in (7) for the estimator $\hat{P}^{(1)} = S$ in presence of thermal noise (red), which is biased when compared to the power of the noiseless signal P_{dBW} (in blue). P_{dBW}^{ref} is the reference power, set by the experimenter.

One problem with the definition of the dynamic range in (7) is that it does not consider the variance of S, but solely its bias $\mathbb{E}[S]$ (see (5)). While this is acceptable for estimators with large biases with respect to their variances (it is the case for S when the signal-to-noise ratio is low, see left part of Fig. 4), this is an issue for less biased estimators (leading to an infinite dynamic range $R_D^{(1)}$ for an unbiased estimator of P). Because the goal of the present paper is precisely to propose an estimator with a bias as low as possible, the dynamic range definition in (7) is modified in three ways: (a) the Root Mean Square Error (RMSE) is used in place of the mean error to take into account the variance of the estimator, (b) the error of the logarithm is used rather than the logarithm of the error, and (c) the quantity to be estimated is the filtered power, as it is usual in propagation studies. In such conditions, (6) becomes:

$$\Delta^{(2)} \overset{\text{def}}{=} \sqrt{\mathbb{E}\left[\left(\widehat{P_{dBW}^{filt}} - P_{dBW}^{filt}\right)^2\right]}, \tag{8}$$

leading to the new dynamic range definition $R_D^{(2)}$, in compliance with (7):

$$\begin{aligned} R_D^{(2)} &\overset{\text{def}}{=} \max\left\{\widehat{A_{dB}}(t)\right\} \,\middle|\, \Delta^{(2)} < \Delta_{max}^{(2)}, \\ &= \max\left\{P_{dBW}^{ref}(t) - \widehat{P_{dBW}^{filt}}(t)\right\} \,\middle|\, \Delta^{(2)} < \Delta_{max}^{(2)} \end{aligned} \tag{9}$$

where $\Delta_{max}^{(2)}$, in dB, is the maximum error tolerated by the user of the beacon data.

Because the reference power P_{dBW}^{ref} is generally not constant (it fluctuates due to movements of the satellite, drifts of the receiver, attenuation from atmospheric gases, scintillation effects…), the dynamic range might actually change with respect to time. However, as mentioned previously, when extracting attenuation from beacon measurements, fast signal fluctuations related to scintillation effects are commonly partly removed by low-pass filtering (see Section IV.B). As for the other effects, they are expected to be quite low (typically less than 1 or 2 dB throughout a day [8]). Lastly, it has to be noted that the dynamic range is not only affected by the characteristics of the beacon receiver, but also by the characteristics of the satellite (mainly its EIRP, and marginally on the characteristics of the signal sent, such as its phase noise, or the Doppler shift of the carrier frequency). The climatological differences between locations should also play a role (sky noise power depends on its physical temperature and dynamics of gaseous attenuation depend on the location), but are assumed to be of second order.

IV. Noise Corrections By Minimising The Estimation Bias

As mentioned in Section III, due to the presence of thermal noise originating from the sky and from the receiver components, the noisy power S_{dBW} at the output of a beacon receiver is a positively biased estimator $\widehat{P_{dBW}}^{(1)}$ of the noiseless power P_{dBW}. Therefore, this section is dedicated to the definition and the mathematical derivation of the statistical properties of two estimators, $\widehat{P_{dBW}^{filt}}^{(2)}$ *and* $\widehat{P_{dBW}^{filt}}^{(3)}$, that both reduce the estimation bias (i.e. the noise contribution). They both rely on the estimation of the noise power σ_S^2 in the beacon frequency band B_S. To do so, an estimator $\widehat{N_0}$ of the noise power spectral density N_0 is first required. This estimator $\widehat{N_0}$ is defined from power measurements in the adjacent frequency band B_N.

A. Noise Spectral Density Estimation

Let i be an integer, T_S the sampling period of the ADC in Fig. 1 and $v_N(i \cdot T_S)$ the I/Q samples after going through the band-pass filter in Fig. 2, which isolates the spectral components solely due to thermal noise in the adjacent frequency band. The samples $v_N(i \cdot T_S)$ are a root-power quantity (a voltage or a current, up to a multiplicative constant). In compliance with Fig. 5, from the discrete summation of the square of the modulus of $v_N(i \cdot T_S)$ over the integration time T_I, the receiver provides an estimator N of the noise power σ_N^2 in the adjacent frequency band:

$$N(k \cdot T_I) \overset{\text{def}}{=} \frac{1}{r} \sum_{i=k \cdot r}^{(k+1)\cdot r - 1} |v_N(i \cdot T_S)|^2, \tag{10}$$

where $r = T_I/T_S$ is the number of I/Q samples (right after the ADC) over the integration time T_I. N could alternatively be computed in the Fourier frequency domain, with equivalent results, in virtue of Parseval's theorem.

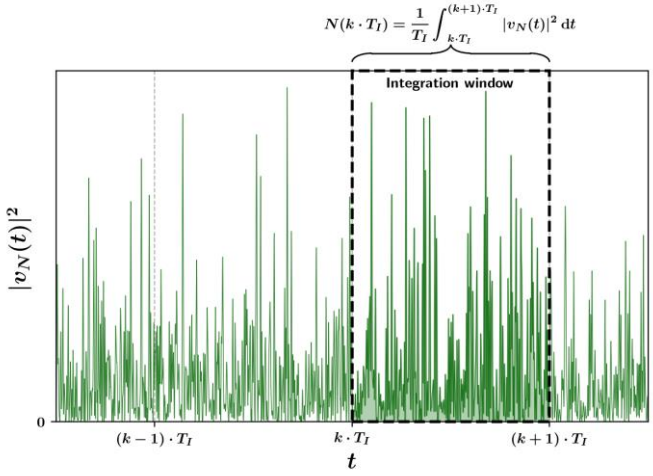

Fig. 5. Beacon receiver estimation $N(k \cdot T_I)$ of the noise power σ_N^2 from the integration of the square of the modulus of $v_N(i \cdot T_S)$ produced by the ADC in Fig. 2 over the interval $k \cdot T_I \leq t \leq (k+1) \cdot T_I$.

Under the AWGN assumption, the samples $v_N(i \cdot T_s)$ are normally distributed, with a variance equal to the noise power σ_N^2 in the adjacent frequency band. Although σ_N^2 is likely to change over time (for instance due to variations of the sky brightness temperature), it is assumed that over the beacon integration time T_I (typically less than a second) the noise is stationary. In such conditions, the samples $v_N(i \cdot T_s)$ follow a normal law:

$$v_N \sim \mathcal{N}(0, \sigma_N^2). \tag{11}$$

Now, let m be the time-bandwidth product:

$$m \stackrel{\text{def}}{=} B_N \cdot T_I \tag{12}$$

where m is supposed to be an integer (it is the case for brickwall filters implemented using the Discrete Fourier Transform DFT). In compliance with [19], the distribution of the power of a band-limited, AWGN follows a chi-square (χ^2) distribution with a number of degrees of freedom equal to twice the time-bandwidth product m. Therefore, from (10), the distribution of N follows a chi-square distribution:

$$N \sim \frac{\sigma_N^2}{2m} \chi^2(2m), \tag{13}$$

and its Probability Density Function (PDF) f_N is given by:

$$f_N(x) = \frac{x^{m-1} e^{-\frac{m}{\sigma_N^2} \cdot x}}{\Gamma(\mathrm{m}) \left(\frac{\sigma_N^2}{m}\right)^m}, \tag{14}$$

where Γ is the gamma function.

From (13) and [20], the expected value $\mathbb{E}[N]$ and the variance $var(N)$ of the estimator N are given by:

$$\mathbb{E}[N] = \sigma_N^2, \tag{15}$$

and

$$var(N) = \frac{\sigma_N^4}{m}. \tag{16}$$

Equation (15) shows that N is an unbiased estimator of the noise power σ_N^2 in the band B_N. Equation (16) indicates that N estimates all the better σ_N^2 as m increases (i.e. as the measurement bandwidth B_N or the integration time T_I increases). In practice, T_I is low (less than 1s) while B_N can be large (several kHz, see Table II), as the frequency bands adjacent to the beacon frequency band are usually guard bands, i.e. free of signals.

Now, the noise power spectral density N_0 is commonly expressed from the noise power σ_N^2 in the adjacent frequency band:

$$N_0 \stackrel{\text{def}}{=} \frac{\sigma_N^2}{B_N}, \tag{17}$$

so that using (15), the expected value $\mathbb{E}[N]$ of the estimator N is related to N_0 through:

$$\mathbb{E}[N] = N_0 \cdot B_N. \tag{18}$$

Assuming that N is stationary over time periods longer than T_I, l consecutive samples of N can be used to estimate the noise power density N_0. In these conditions, the maximum likelihood estimator $\widehat{N_0}$ of the noise power spectral density is the empirical mean of the samples $N(k \cdot T_I)$:

$$\widehat{N_0}(k \cdot T_I) \stackrel{\text{def}}{=} \frac{1}{l \cdot B_N} \sum_{i=0}^{l-1} N[(k+i) \cdot T_I]. \tag{19}$$

Although equations (10) and (19) could be performed in a single step, in practice, the I/Q samples are not stored directly, as this operation would require too much storage capacity in the receiver. Instead, the samples $N(k \cdot T_I)$ are stored with a sampling period T_I, requiring that the estimation driven by (19) is computed in two separate steps.

Considering independent and identically distributed random variables, it follows from (18) and (19) that:

$$\begin{aligned} \mathbb{E}\left[\widehat{N_0}\right] &= \frac{\mathbb{E}[N]}{B_N} \\ &= N_0, \end{aligned} \tag{20}$$

and

$$\begin{aligned} var\left(\widehat{N_0}\right) &= \frac{l \cdot var(N)}{(l \cdot B_N)^2} \\ &= \frac{\sigma_N^4}{l \cdot m \cdot B_N^2} \\ &= \frac{N_0^2}{B_N \cdot T_I \cdot l}. \end{aligned} \tag{21}$$

Under the hypothesis of stationarity of the noise, (20) shows that $\widehat{N_0}$ in (19) is an unbiased estimator of N_0 while (21) indicates that the noise power spectral density estimator $\widehat{N_0}$ has a lower variance as the product $B_N \cdot T_I \cdot l$ increases. Particularly, increasing l produces better estimates of N_0. However, if l is too large, the hypothesis of stationarity of the signal might not hold. From empirical measurements (a few tens of GHz, with antenna sizes of roughly 1 m), it was determined that over periods of 10 seconds, the noise power remains nearly constant (i.e. $l \cdot T_I = 10\,s$ should be acceptable to estimate the noise spectral power density).

B. Signal Power Estimation

1) Description of the method to derive the estimators

As mentioned in Section III, attenuation time series $\widehat{A_{dB}}(t)$ are derived from beacon receivers using (2), where the reference power P_{dBW}^{ref} is fixed by the experimenter. Therefore, it remains to estimate the quantity P_{dBW}^{filt}, which contains the low frequency components of the ideal, noiseless power P_{dBW}, mainly caused by tropospheric attenuation effects. Usually, the low-pass filtered, noisy power S_{dBW}^{filt} measured by the beacon receiver is used as a first estimate $\widehat{P_{dBW}^{filt}}^{(1)}$ (the customary estimator) of P_{dBW}^{filt} [2].

Nevertheless, $\widehat{P_{dBW}^{filt}}^{(1)} = S_{dBW}^{filt}$ is a biased estimator overestimating the filtered noiseless power P_{dBW}^{filt}. Consequently, this standard process that ignores noise power, though widely used in the propagation community, leads to an underestimation of A_{dB}. This underestimation is stronger as the signal-to-noise ratio is low (i.e. as the attenuation is high).

Therefore, in the next subsections, two estimators $\widehat{P_{dBW}^{filt}}^{(2)}$ and $\widehat{P_{dBW}^{filt}}^{(3)}$ are proposed. Precise estimation methods (such as maximum likelihood estimation) would require an expression of the probability density function of S_{dB}^{filt}, which

is unknown. As a consequence, the method of moments is used to derive these estimators, which solely requires an expression of the expected value of S_{dBW}^{filt}. Finding $\mathbb{E}[S_{dBW}^{filt}]$ is the object of subsections IV.B.2) through IV.B.4).

2) Definition of the noisy power S measured by the beacon receiver

Analogous to (12), let n be the time-bandwidth product in the beacon frequency band:

$$n \stackrel{\text{def}}{=} B_S \cdot T_I. \tag{22}$$

n is assumed to be an integer (it is the case if the filter to isolate the beacon frequency band is a brick-wall filter implemented using the DFT).

The power of the noisy signal $S(k \cdot T_{int})$ measured by the beacon receiver results from the discrete integration of the square of the modulus of the complex samples v_S (cf. Fig. 2):

$$S(k \cdot T_I) \stackrel{\text{def}}{=} \frac{1}{r} \sum_{i=k \cdot r}^{(k+1) \cdot r - 1} |v_S(i \cdot T_s)|^2, \tag{23}$$

where, as before, k is the index of the samples S and $r = T_I / T_S$.

As stated in Section II, thermal noise is modelled as an AWGN. Consequently, the measured signal $v_S(t)$ can be decomposed into the sum of the noiseless signal $v_P(t)$ with a white, Gaussian noise $v_{N'}(t)$ (the prime being used to differentiate the noise contribution $v_{N'}(t)$ in the beacon frequency band from $v_N(t)$ in section IV.A that refers to the noise in the adjacent frequency band B_N):

$$v_S(t) = v_P(t) + v_{N'}(t), \tag{24}$$

and

$$v_{N'}(t) \sim \mathcal{N}\left(0, \sigma_S^2(t)\right). \tag{25}$$

Similarly, the power P in the absence of sources of thermal noise, integrated over T_I, expressed in watts, is defined as

$$P(k \cdot T_I) \stackrel{\text{def}}{=} \frac{1}{r} \sum_{i=k \cdot r}^{(k+1) \cdot r - 1} |v_P(i \cdot T_s)|^2. \tag{26}$$

Although P is unknown, it is considered a parameter (i.e. it is not a random variable). Fig. 6 illustrates S and P defined by equations (23) and (26) for two different signal-to-noise ratios. When the signal-to-noise ratio is high (red dashed curve), S is rather close to P. On the other hand, if the signal-to-noise ratio is low, S strongly overestimates P. As previously stated, S_{dBW} is also expected to be a positively biased estimator of P_{dBW}.

3) Derivation of the expected value of S

As shown in [21], since the samples $v_{N'}$ are normally distributed with variance σ_S^2 in compliance with (25), then S in (23) follows a non-central chi-square (χ_{nc}^2) distribution with $2n$ degrees of freedom, and a non-centrality parameter equal to the ratio of signal power to the noise power spectral density:

$$S \sim \frac{\sigma_S^2}{2n} \cdot \chi_{nc}^2 \left(2n, \frac{2n}{\sigma_S^2} P\right). \tag{27}$$

Consequently, the PDF of S is given by

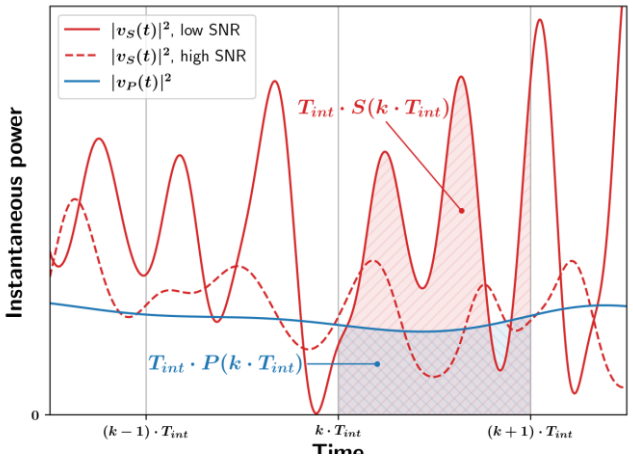

Fig. 6. Illustration of the power measured by the beacon receiver from the integration of the instantaneous power $v_p(t)$ over T_I seconds, for two values of the signal-to-noise ratio (plain red line: a signal-to-noise ratio of 0 dB, dashed red line: a signal-to-noise ratio of 10 dB). The blue curve is the noiseless power that would measure an ideal beacon receiver in the absence of thermal noise.

$$f_S(x) = \frac{2n}{\sigma_S^2} \cdot \chi_{nc}^2 \left(\frac{2n}{\sigma_S^2} x; 2n, \frac{2n}{\sigma_S^2} P\right), \tag{28}$$

where $\chi_{nc}^2(\cdot; k, \lambda)$ is the non-central chi-square PDF, defined as

$$\chi_{nc}^2(t;\ k, \lambda) \stackrel{\text{def}}{=} \frac{e^{-\frac{\lambda + t}{2}}}{2} \cdot \left(\frac{t}{\lambda}\right)^{\frac{k}{4} - \frac{1}{2}} \cdot I_{\frac{k}{2}-1}\left(\sqrt{\lambda t}\right), \tag{29}$$

where $I_{\frac{k}{2}-1}$ is the modified Bessel function of the first kind, which order is $\frac{k}{2} - 1$.

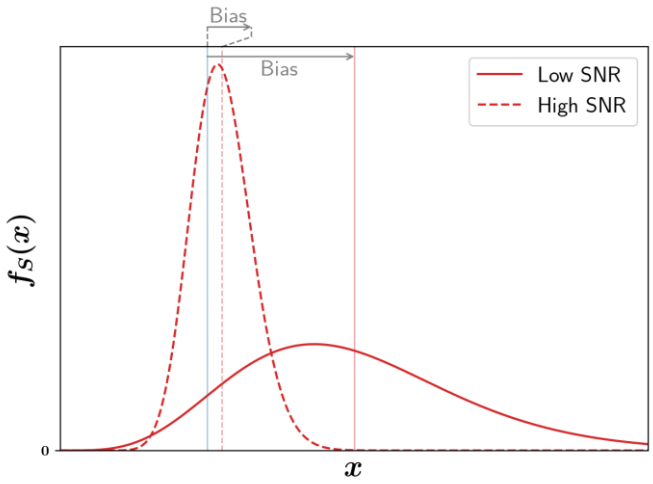

Fig. 7. PDF $f_S(x)$ of the power S in the beacon frequency band given by (28), for two values of the signal-to-noise ratio (plain red line: 0 dB, dashed red line: 10 dB), for $n = 5$, along with the expected values of the distributions as vertical red lines.

Using (27) and [20], the expected value of S can be expressed as

$$\begin{aligned} \mathbb{E}[S] &= \frac{\sigma_S^2}{2n} \cdot \left(2n + \frac{2n \cdot P}{\sigma_S^2}\right) \\ &= \sigma_S^2 + P, \end{aligned} \tag{30}$$

which is an expected result, the power of two independent signals being the sum of the power of the individual signals. In fact, (30) holds independently of the noise characteristics, provided that it is independent of the signal (in particular, it

does not need to be a Gaussian noise). The PDF of S is plotted in Fig. 7, for two values of the signal-to-noise ratio. In the particular case of a signal-to-noise ratio of 0 dB (i.e. $P = \sigma^2$, shown as a plain red line in Fig. 7), the expected value $\mathbb{E}[S]$ is twice the power of the signal in compliance with (30). For higher values of the signal-to-noise ratio, the bias of S is usually low with respect to its variance (see the dashed curve in Fig. 7).

Because the noise is considered to be white, the power spectral density is constant, therefore:

$$\sigma_S^2 = N_0 \cdot B_S, \tag{31}$$

and (30) becomes:

$$\mathbb{E}[S] = B_S \cdot N_0 + P. \tag{32}$$

4) Derivation of the expected value of S_{dBW}^{filt}

Due to the monotonicity of the logarithm, from (28), the PDF $f_{S_{dBW}}$ of $S_{dBW} \overset{\text{def}}{=} 10\log_{10}(S)$ can be expressed as

$$f_{S_{dBW}}(x) = \frac{2n \cdot \ln(10)}{10\sigma_S^2} \chi^2\left(\frac{2n}{\sigma_S^2} 10^{\left(\frac{x}{10}\right)}; 2n, \frac{2nP}{\sigma_S^2}\right) 10^{\frac{x}{10}}. \tag{33}$$

A closed form of the expected value of the logarithm of a chi-square distribution is given in [22]. Applied on (33), one obtains:

$$\mathbb{E}[S_{dBW}] = 10\log_{10}\left(\frac{\sigma_S^2}{n}\right) + \frac{10}{\ln(10)} g_n\left(\frac{nP}{\sigma_S^2}\right), \tag{34}$$

where g_n is a continuous, strictly increasing function given by:

$$g_n(x) \overset{\text{def}}{=} \begin{cases} \psi(n), & if\ x = 0 \\ \ln(x) - Ei(-x) + \sum_{i=1}^{n-1}\left(-\frac{1}{x}\right)^i \cdot \left(e^{-x}(j-1)! - \frac{(n-1)!}{j(n-1-j)!}\right), & else \end{cases}, \tag{35}$$

with $\psi(\cdot)$ the digamma function and $Ei(\cdot)$ the exponential integral function, defined as

$$Ei(x) \overset{\text{def}}{=} \int_{-\infty}^{x} \frac{e^t}{t} dt. \tag{36}$$

Now, as the low-pass filter to remove scintillation is linear, with a frequency response H, and assuming that $S_{dBW}(t)$ is a stationary random process with power spectral density $\mathcal{S}_{S_{dBW}}(f)$, then the power spectral density of the filtered signal $S_{dBW}^{filt}(t)$ is given by:

$$\mathcal{S}_{S_{dBW}^{filt}}(f) = |H(f)|^2 \cdot \mathcal{S}_{S_{dBW}}(f). \tag{37}$$

In particular, $H(0) = 1$, so it follows that the expected value (the DC component) of S_{dBW}^{filt} is equal to the expected value of S_{dBW} so that, using (34),

$$\begin{aligned} \mathbb{E}\left[S_{dBW}^{filt}\right] &= \mathbb{E}[S_{dBW}] \\ &= 10\log_{10}\left(\frac{\sigma_S^2}{n}\right) + \frac{10}{\ln(10)} g_n\left(\frac{nP}{\sigma_S^2}\right), \end{aligned} \tag{38}$$

The stationarity of S_{dBW} is a questionable hypothesis, as rain or clouds attenuation can change substantially within tens of seconds. Consequently, the performance of the estimators derived in subsection IV.B.5), using this hypothesis will be tested on synthetic data aiming at reproducing actual attenuation dynamics in Section V.

5) Definition of the estimators

From the previous paragraphs, three estimators are proposed.

✓ *"Customary" estimator*

As mentioned in previous sections, the first estimator $\widehat{P_{dBW}^{filt}}^{(1)}$, referred as the customary estimator hereafter, is the estimator generally used in propagation studies when noise measurements are not available:

$$\widehat{P_{dBW}^{filt}}^{(1)} \overset{\text{def}}{=} S_{dBW}^{filt}. \tag{39}$$

As previously discussed, when the signal-to-noise ratio is low, the positive bias associated with $\widehat{P_{dBW}^{filt}}^{(1)}$ is expected to be significant and the actual attenuation is underestimated.

✓ *"Natural" estimator*

An estimator $\hat{P}^{(2)}$, proposed in [4], is derived from the expression of the expected value $\mathbb{E}[S]$ of S in watts in (32), using the method of moments:

$$\hat{P}^{(2)} = S - B_S \cdot \widehat{N_0}. \tag{40}$$

However, since (40) gives negative values if $S < B_S \cdot \widehat{N_0}$, a revised expression is proposed so that (40) becomes:

$$\hat{P}^{(2)\prime} = \begin{cases} S - B_S \cdot \widehat{N_0} & if\ S \geq B_S \cdot \widehat{N_0} \\ 0 & else \end{cases}. \tag{41}$$

After a change of variable $S_{dBW} = 10 \cdot \log_{10}(S)$, the natural estimator $\widehat{P_{dBW}^{filt}}^{(2)}$ of the noiseless power P_{dBW}^{filt} emerges:

$$\widehat{P_{dBW}^{filt}}^{(2)} = S_{dBW}^{filt} + h\left(\frac{10^{\left(\frac{S_{dBW}^{filt}}{10}\right)}}{B_S \cdot \widehat{N_0}}\right), \tag{42}$$

where h is a function given by

$$h(x) \overset{\text{def}}{=} \begin{cases} 10\log_{10}\left(1 - \frac{1}{x}\right) & if\ x > 1 \\ -\infty & else \end{cases}. \tag{43}$$

Because the change of variables is not linear, it is expected that $\widehat{P_{dBW}^{filt}}^{(2)}$ is a biased estimator of P_{dBW}^{filt}.

✓ *"Logarithmic" estimator*

Instead, using the method of moments directly on the expected value of S_{dBW}^{filt} should give a less biased estimator. Inverting (38) gives the logarithmic estimator:

$$\begin{aligned} \widehat{P_{dBW}^{filt}}^{(3)} &= \frac{\sigma_S^2}{n} \cdot g_n^{-1}\left[\frac{\ln 10}{10}\left(S_{dBW} - 10\log_{10}\left(\frac{\sigma_S^2}{n}\right)\right)\right] \\ &= S_{dBW}^{filt} + h_n\left(\frac{10^{\left(\frac{S_{dBW}^{filt}}{10}\right)}}{B_S \cdot \widehat{N_0}}\right), \end{aligned} \tag{44}$$

where h_n is defined as

$$h_n(x) \overset{\text{def}}{=} \begin{cases} 10\log_{10}\left(\dfrac{g_n^{-1}[\ln(nx)]}{nx}\right) & if\ x > \dfrac{e^{\psi(n)}}{n} \\ -\infty & else \end{cases}. \quad (45)$$

The value $-\infty$ for x smaller than $e^{\psi(n)}/n$ is obtained by analytic continuation of h_n, and is consistent with the expected behaviour of h_n: a measured power lower than the noise floor is most likely caused by a null power from the beacon, i.e. $-\infty$ dB. From an experimenter point of view, this infinite value is not an issue, as attenuation values exceeding the dynamic range (that remains to be set) are generally marked as unreliable. A practical implementation of g_n^{-1} is proposed in Appendix A.

Intuitively, the functions h and h_n, plotted in Fig. 8, correspond to the corrections applied to S_{dBW}^{filt} (that is, again, commonly used to estimate P_{dBW}^{filt}) to obtain respectively the natural $\widehat{P_{dBW}^{filt}}^{(2)}$ and logarithmic $\widehat{P_{dBW}^{filt}}^{(3)}$ estimators. In compliance with Fig. 8, the corrections applied to S_{dBW}^{filt} are substantial, especially when n is higher than 1: it can amount to several dB for low values of the signal-to-noise ratio. On the contrary, for high values of the signal-to-noise ratio, the corrective functions h and h_n approach 0 dB. Besides, as shown in Appendix B, the functions h and h_n are asymptotically equal as n tends towards infinity. In other words, $\widehat{P_{dBW}^{filt}}^{(2)}$ in (42) becomes increasingly close to $\widehat{P_{dBW}^{filt}}^{(3)}$ in (44) when increasing the measurement bandwidth B_S, i.e. when n increases in compliance with (22).

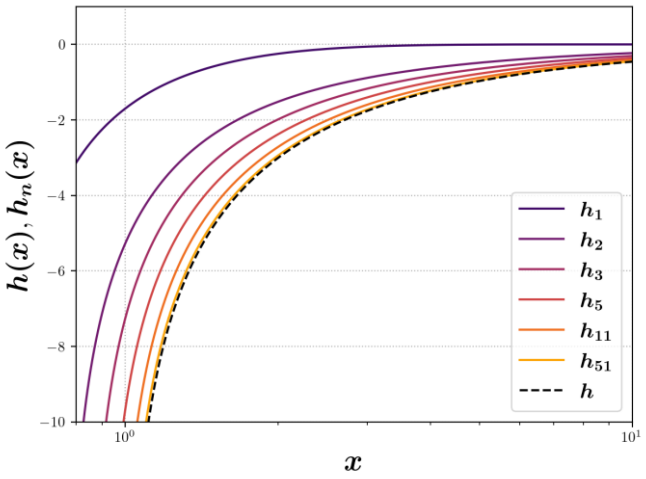

Fig. 8. The correction functions h and h_n, for a few values of n (1, 2, 3, 5, 11, 51).

V. Performance of the Estimators

The estimators previously defined have been derived assuming S_{dBW} is a stationary process. However, this hypothesis is questionable, since attenuation can change drastically within seconds. Consequently, the performances of the customary $\widehat{P_{dBW}^{filt}}^{(1)}$, natural $\widehat{P_{dBW}^{filt}}^{(2)}$ and logarithmic $\widehat{P_{dBW}^{filt}}^{(3)}$ estimators are assessed from simulations of synthetic time series of total tropospheric attenuation associated with the beacon receiver model described in Section II.

A. Synthetic Time Series Generation

Synthetic time series of total tropospheric attenuation $A_{dB}^{tot}(t)$ have been generated using Recommendation ITU-R P.1853-2 [23]. Since experimental beacon data collected at Ka and Q bands in Toulouse (South-West of France) will be used in Section VII, the selected beacon frequency is $f_b = 39.4\,GHz$ and Rec. ITU-R P.1853-2 is used from the geographical coordinates of Toulouse. For simulation purposes, the signal and noise powers are computed at the input of the beacon receiver (right after the antenna in Fig. 1), while the noise generated by the receiver is virtually brought back to the input of the receiver in order to avoid having unnecessary characteristics of the receiver in the following equations (such as the gain of the receiving chain) [24].

The synthetic time series of noiseless power level $P_{dBW}(t)$ (in dBW) and $P(t)$ (in watts) at the input of the beacon antenna are computed according to:

$$P_{dBW}(t) = P_{dBW}^{ref} - A_{dB}^{tot}(t), \quad (46)$$

and

$$P(t) = 10^{P_{dBW}(t)/10}, \quad (47)$$

where P_{dBW}^{ref} is the reference power that would be received in the absence of atmosphere (since, in this case, total attenuation is considered). P_{dBW}^{ref} is assumed constant (ignoring variations induced by movements of the satellite or drifts of the RF chain), and is fixed arbitrarily, so that the signal-to-noise ratio in clear sky conditions is equal to 32 dB, i.e. a value similar to the one of the Q-band receiver considered in Section VII. Taking values for the parameters similar to the ones of the experimental beacon receiver will ease comparisons afterwards.

The equivalent noise temperature generated by the receiver, measured at the input of the receiver, is by definition:

$$T_r = T_0(F - 1), \quad (48)$$

where T_0 is the reference temperature (290 K), and F the noise figure of the receiver defined in Table I.

The sky brightness temperature at the input of the receiver, is given by [25]:

$$T_b(t) = T_{mr}([1 - A'(t)]) + 2.7A'(t), \quad (49)$$

where $A'(t)$ (unitless) is the total atmospheric attenuation (gases, clouds and rain) excluding scintillation, averaged over the radiation pattern of the receiving antenna. $T_{mr} = 275K$ is the effective mean radiating temperature of the sky. Assuming the LNB is located just after the antenna feeder to avoid noticeable loss from the cables, and the receiving antenna is sufficiently directive to neglect noise originating from the ground, the total effective noise temperature, at the input of the receiver, is

$$T_e(t) = T_b(t) + T_r, \quad (50)$$

and the noise power in the beacon receiver band is finally given in watts by:

$$\sigma_S{}^2(t) = kT_e(t)/T_s, \quad (51)$$

where k is the Boltzmann constant and T_s is still the ADC sampling period.

It has to be noted that, strictly speaking, attenuation times series measured by a beacon receiver are only affected by the

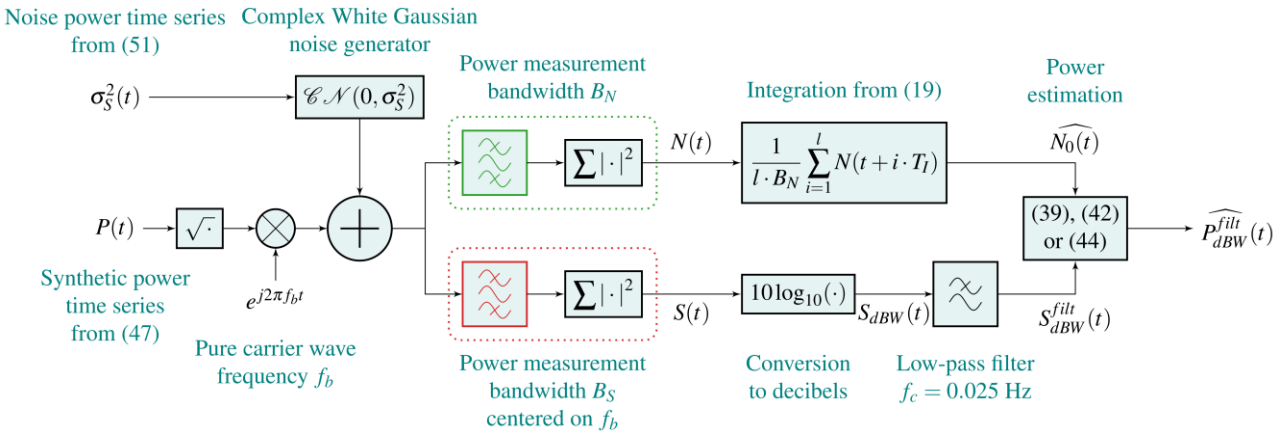

Fig. 9. Block diagram of the numerical implementation of the beacon receiver model.

propagation medium in a small area (essentially equal to the first Fresnel zone of the link), whereas the power of the noise is impacted by a larger portion of the sky (the beam width of the antenna). This distinction should have little effects considering the high directivity of the antenna, and should act as a worst-case scenario: in practice, variations of the noise temperature should be lower, so the hypothesis of stationarity of the noise power spectral density should hold even more.

B. *Beacon Receiver Model*

The generic beacon receiver described in Section II has been implemented numerically according to the block diagram in Fig. 9. The parameters are given in Table I. They are identical to the parameters of the experimental receivers presented in Section VII.

TABLE I
PARAMETERS OF THE BEACON RECEIVER MODEL

B_N	B_S	T_I	F	l
25 kHz	50 Hz	0.1 s	2 dB	100

From Table I and (22), the value of the parameter n is 5. The value of l has been fixed to obtain an effective integration time for the estimation of the noise power spectral density of $l \times T_I = 10$ seconds. This is a conservative value, considering that the sky noise temperature evolves generally slowly, as it is integrated over the radiation pattern of the receiving antenna. Also, experimental data at Ka and Q bands have shown that the noise power spectral density is almost constant over time periods of a few seconds.

The band-pass filters that isolate the beacon frequency band (in red in Fig. 9) and the adjacent frequency band (in green in Fig. 9) are brick-wall filters implemented using the DFT. The low-pass filter used to remove scintillation is a forward-backward Butterworth filter of 3rd order (effective 6th order), with a cut-off frequency of 0.025 Hz.

Fig. 10 shows time series of excess attenuation generated using ITU-R P.1853-2 (dashed, black line P_{dBW}^{filt}), along with simulated beacon receiver data in presence of thermal noise (thin blue line S_{dBW}), and the three estimators (customary, natural and logarithmic) defined in Section IV.B.5). The noise power in the frequency band of the beacon is shown as a red line. When the signal-to-noise ratio is high (e.g. between 0 and 3 minutes), all three estimators are accurate. For a signal-to-noise ratio close to unity (between 4 and 8 minutes, or around 14 minutes), the customary estimator $\widehat{P_{dBW}^{filt}}^{(1)}$ is clearly overestimating the power level, the natural estimator $\widehat{P_{dBW}^{filt}}^{(2)}$ tends to slightly underestimate the power level, while the logarithmic estimator $\widehat{P_{dBW}^{filt}}^{(3)}$ is accurate. Now, when the power of the signal is significantly lower than the power of the noise (between 9 and 12 minutes), none of the estimators are accurate. In particular, the natural and logarithmic estimators output infinite values.

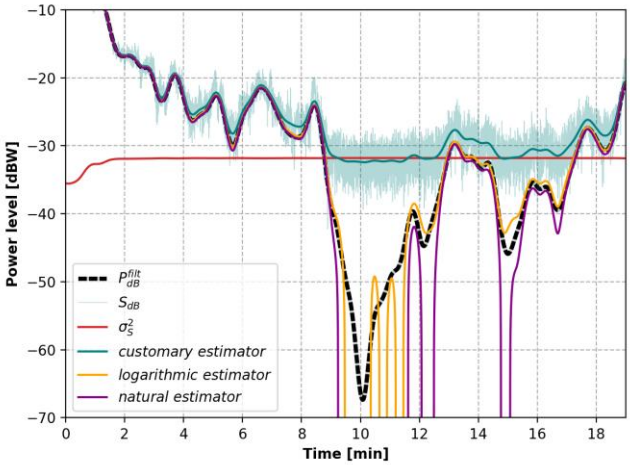

Fig. 10. Synthetic rainy event generated using ITU-R P.1853, along with the three estimators.

C. *Root Mean Square Error of the Estimators*

The generic error figure for beacon power time series is the Root Mean Square Error (RMSE) $\Delta^{(2)}$ defined in (8).

As the total attenuation synthesizer in Rec. ITU-R P.1853-2 is based on a mixed dirac-lognormal approach, it is necessary to generate a large database of tropospheric attenuation in order to get high attenuation values (which happen with a low probability), close to the beacon receiver saturation. It was found that 20 years of synthetic data is sufficient for the RMSE to converge (or, in other words, to obtain smooth curves).

Fig. 11 gives the RMSE of the three estimators previously defined, as a function of the carrier-to-noise density ratio C/N_0. As shown in Appendix C, the RMSE of the estimators only depends on the signal-to-noise ratio (or equivalently the signal-to-noise density ratio C/N_0, as the receiver bandwidth is constant). The customary estimator has the highest error. In comparison, the natural estimator shows significant improvements: for an acceptable error level $\Delta^{(2)}$ of 1 dB, the dynamic range is increased by about 7 dB. The logarithmic estimator, although more complex, is even more precise: for

the same level of error, it increases the dynamic range by about 12 dB. The bias $\Delta^{(1)}$ given by (5) is plotted as a dashed black curve. It is higher than the RMSE of the customary estimator, due to its definition using the power level in watts, rather than dBW.

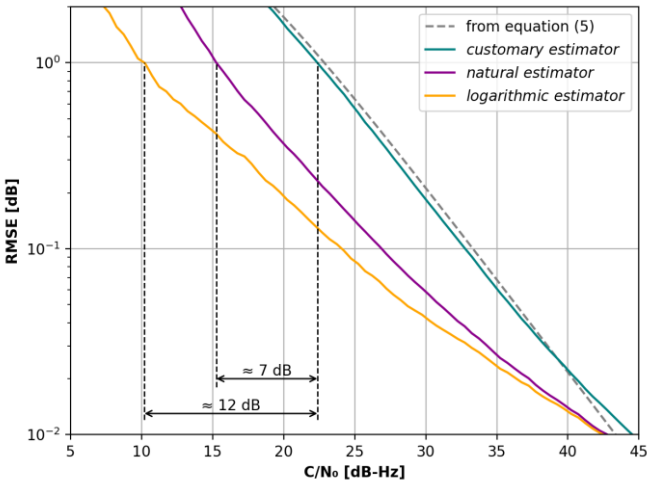

Fig. 11. RMSE $\Delta^{(2)}$ of the three estimators (plain curves), simulated with 20 years of synthetic data, as well as the bias $\Delta^{(1)}$, according to (5) for $n = 5$ (see Table I and (22)).

D. Application of the Estimators to Distributions of Attenuation

The same estimators can be used to compute Complementary Cumulative Distribution Functions (CCDFs) of excess attenuation. Fig. 12 shows the CCDF of excess attenuation computed from the simulated synthetic time series (the 'true' CCDF computed from noiseless time series $P_{dBW}^{filt}(t)$ as a dashed black line, and the CCDFs derived from the three estimated time series $\widehat{P_{dBW}^{filt}}^{(1)}(t)$, $\widehat{P_{dBW}^{filt}}^{(2)}(t)$ and $\widehat{P_{dBW}^{filt}}^{(3)}(t)$ in presence of noise as coloured lines). As expected, for low attenuations (high signal-to-noise ratio), all the estimators yield CCDFs identical to the one of the noiseless signal. It can be seen that using the customary estimator, there is a saturation effect: the attenuation cannot exceed a value (here about 32 dB) determined by the noise floor of the receiver. Using the natural estimator, a large part of the bias is removed, leading to a CCDF closer to the one of the noiseless synthetic signal. Finally, the logarithmic estimator yields a CCDF that is almost indistinguishable from the one using a noiseless receiver, up to attenuation levels 10 dB above the noise floor (a signal-to-noise ratio of approximately -10 dB).

VI. Effect of the Bandwidth

Because of several unwanted effects, such as the Doppler shift, as well as the frequency stability of the clocks of the satellite and of the receiver, the beacon carrier frequency f_b might change quite significantly over a day. For instance, [26] presents a beacon receiver using the satellite Alphasat, with frequency variations of more than 1 kHz over a day. Consequently, the carrier frequency must be estimated, which is the subject of many papers in the literature, such as [27]. In fact, several frequency estimation algorithms exist, with a significant impact on the dynamic range of the receiver.

One way to counteract the impact of noise estimation errors is to increase the measurement bandwidth of the receiver (B_S)

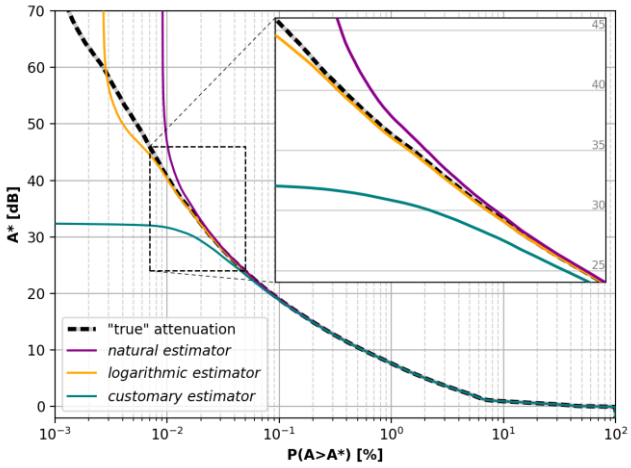

Fig. 12. CCDFs of excess attenuation from the noiseless synthetic time series (ideal receiver) generated using ITU-R P.1853, and from the three estimators in presence of thermal noise (actual receiver).

[27]. However, when only the measurement in the beacon frequency band is used, increasing the measurement bandwidth will reduce the signal-to-noise ratio and therefore the dynamic range of the receiver. Consequently, the parameter n, proportional to the bandwidth B_S (see (22)), is chosen as a trade-off between the signal-to-noise ratio in the beacon frequency band, and the impact of frequency estimation errors. In Section V, n was set to 5 in compliance with Table I. Now, Fig. 13 shows the carrier to noise spectral density ratio C/N_0 required to obtain an RMSE $\Delta^{(2)}$ lower than 1dB, for n ranging from 1 to 51. Note that for $n = 5$, Fig. 13 is consistent with the values of C/N_0 for $\Delta^{(2)} = 1$ dB in Fig. 11. When n is equal to one, the customary estimator $\widehat{P_{dBW}^{filt}}^{(1)}$ requires a C/N_0 nearly 3 dB higher than the logarithmic estimator $\widehat{P_{dBW}^{filt}}^{(3)}$. However, considering the uncertainties of the beacon frequency (f_b) estimation, actual beacon receivers usually opt for values of n higher than 1, so that the beacon frequency remains inside the beacon frequency band. For increasing values of n, the C/N_0 required for the same level of error rapidly increases, whereas for the logarithmic estimator, it is quite contained. For instance, increasing n from 1 to 5 would increase the required C/N_0 by more than 10 dB when considering the customary estimator (effectively decreasing the dynamic range by the same value), whereas using the logarithmic estimator only results in an increase in the required C/N_0 of less than 3 dB (see Fig. 13). For that reason, the value of the receiver bandwidth B_S maximizing the dynamic range of the beacon receiver will be higher when using the logarithmic estimator, rather than the customary estimator. Especially, considering that actual beacon signals are not perfectly pure carriers (due to phase noise, and even more if the signal of the beacon is modulated), increasing the measurement bandwidth would increase the power of the signal in the frequency band of interest. For beacon signals occupying a large enough frequency band, one could even expect that the required C/N_0 actually decreases for increasing measurement bandwidths, although that remains to be proven on actual beacon receivers.

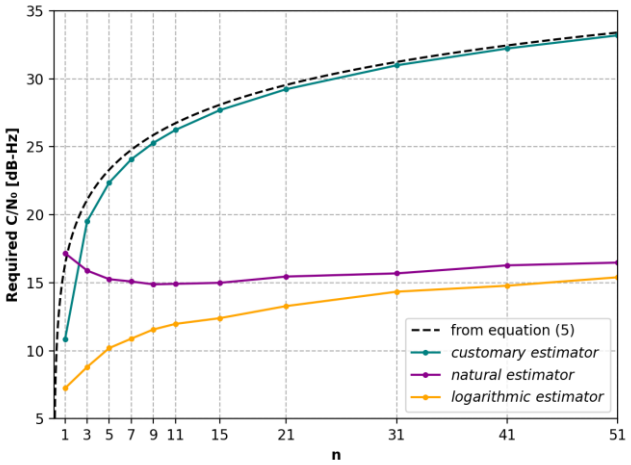

Fig. 13. Required carrier-to-noise-density ratio for an RMSE $\Delta^{(2)}$ lower than 1 dB, as a function of the parameter n. The RMSE of the estimators are derived from synthetic time series of tropospheric attenuation (ITU-R P.1853).

VII. Application to Beacon Receiver Measurements

In this section, the procedure to obtain excess attenuation time series using the three estimators is now illustrated on actual beacon receiver data measured by a Ka-band receiver (Astra 3B, 20.2 GHz beacon) and a Q-band receiver (Alphasat, 39.4 GHz beacon). Both are situated in Toulouse. These receivers are presented in details in [28]. More than 7 years of measurements are available at both frequencies. The two receivers share the same characteristics, as summarized in Table II.

TABLE II
Characteristics of the two experimental beacon receivers

	Carrier frequency	T_I	B_S	B_N
Ka band	39.4 GHz	0.1 s	50 Hz	25 kHz
Q band	20.2 GHz			

The two beacon receivers record power measurements in the beacon frequency band B_S, and in the adjacent frequency band B_N. The beacon receivers do not keep the I/Q symbols in memory, as they would represent a volume of data too high to be stored permanently. Fig. 14 shows the power level during a deep fade event at Q-band (in dB), relatively to a power reference intrinsic to the receiving chain (which actual value in unimportant, as it cancels out when computing attenuation in (1)). The power level measured in the beacon frequency band is displayed as a greenish-blue line S_{dBW}, along with its low-pass filtered version (bold line S_{dBW}^{filt}). The noise power, normalised to be computed on the same bandwidth is plotted in red. The first point to notice is the discontinuity at the end of the event (around 2:41). This is due to a loss of lock, which would prevent from using the estimators previously defined (the attenuation would be overestimated around 2:40). This lock of loss happened for two reasons: (a) the Alphasat satellite has a slightly inclined and eccentric orbit, resulting in a relatively high Doppler frequency shift, and (b) the deep fade rain event is rather long, so when the signal emerges from the noise, the carrier frequency has drifted outside the beacon frequency band, therefore it takes a few seconds for the receiver to lock back to the carrier frequency. Nevertheless, deep fade events with such durations happen rarely, and only a few of these events actually resulted in a loss of lock (there were only two loss of lock during the 7 years of the experiment). The receiver at Ka

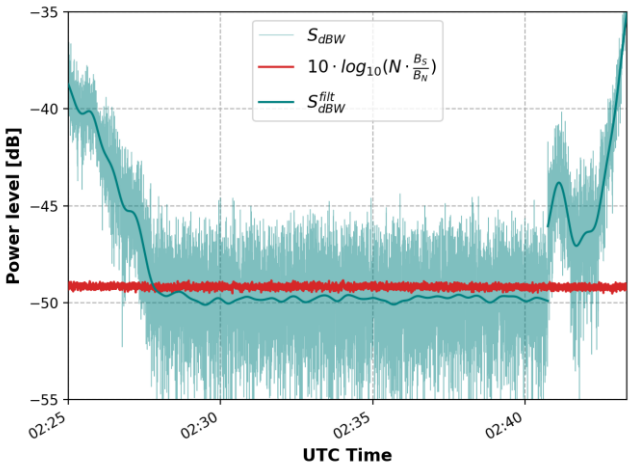

Fig. 14. Example of a deep fade rain event at Q band, collected on the 20th of July, 2018, in Toulouse, with the measured signal S_{dBW} in blue, S_{dBW}^{filt} at the output of a low-pass filter in blue bold, and the normalized noise level in red.

band never lost lock (because deep fade events are shorter, while the Doppler shift of the satellite Astra 3B is lower as it is kept in geostationary position). Generally, an experimenter must be careful that the carrier is always in lock, otherwise the power estimation technique is not applicable.

The second thing to notice on Fig. 14 is that the filtered beacon signal S_{dBW}^{filt} and the normalized noise power are not at the same level during the deep fade event. This indicates that the noise is not perfectly white. Indeed, a true white noise has by definition a flat power spectral density, so in the absence of a signal, the power normalized by the bandwidth should be the same in the useful signal frequency band and in the noise adjacent frequency band. This has been attributed to the analogic filters of the RF chain, as it is common that these filters do not always have a perfectly flat frequency response (e.g. in [6]). Consequently, the estimation of the noise power density $\widehat{N_0}$ driven by (19) in the adjacent frequency band is not applicable as such to the beacon frequency band. Nevertheless, with the less restrictive hypothesis that the noise power spectral density is constant with respect to time (in other words, the frequency response of the analogic filters of the receivers do not change with respect to time, and the Doppler shift does not induce variations of the gain of the receiving RF chain), it is possible to infer the difference of noise power density between the two frequency bands. For the two beacon receivers of this paper, this difference can be measured by comparing the values of S_{dBW} (or equivalently S in natural units) to the normalised noise power during deep fade events. Indeed, when the atmospheric attenuation is very high, the signal of the beacon can be considered absent, leaving the measurements solely affected by thermal noise.

During deep fade events, the difference δ can then be computed in natural units (i.e. not in dB) using the following equation:

$$\delta \overset{\text{def}}{=} \frac{\mathbb{E}[S] \cdot B_N}{\mathbb{E}[N] \cdot B_S}. \tag{52}$$

In order to measure δ for each receiver, several deep fade rain events have been identified during the 7 years of experiment. At Q-band, the receiver saturates for about 0.02% of the time whereas at Ka-band, the receiver saturates

for about 0.003% of the time. This difference is explained by the higher tropospheric attenuation at Q-band with respect to Ka-band, but also by the lower dynamic range of the Q-band receiver with respect to the Ka-band one. At Q-band, 18 deep fade events of more than 10 minutes were visually identified (shorter deep fade events were not kept, as it is harder to precisely identify the beginning and the end of the deep fade). At Ka-band, no deep fade event was long enough to mask the signal of the beacon during 10 minutes over the 7 years. Consequently, deep fade events with durations above 5 minutes have been considered, resulting in the identification of 6 deep fade events. The values of δ_i (i corresponding to the index of the deep fade events) in dB are shown in Fig. 15, each dot corresponding to a deep fade event at Ka (blue) or Q (red) band. The average values of δ_i at Ka and Q band, weighted by the duration of each event, are shown as dashed lines. Additionally, the theoretical standard deviation (equivalent to a 68% confidence interval) of the value δ_i is displayed as error bars. At Q-band, the δ_i values are stable over the 7 years. Their weighted average (red dashed line) is most of the time in the confidence intervals, indicating that δ is likely constant, and the weighted average is a good candidate. At Ka-band, the δ_i values are not as stable. Most importantly, the weighted average (blue dashed line) is not in the confidence intervals of the individual samples. Nevertheless, it is not clear whether it is due to the identification of deep fade events (the signal could still be slightly present), or to drifts of the frequency response of the analog part of the receiver, making δ change with respect to time. Overall, the variations of the δ_i values are quite small (about 0.1 dB), so one could expect little impact on the performance of the estimators.

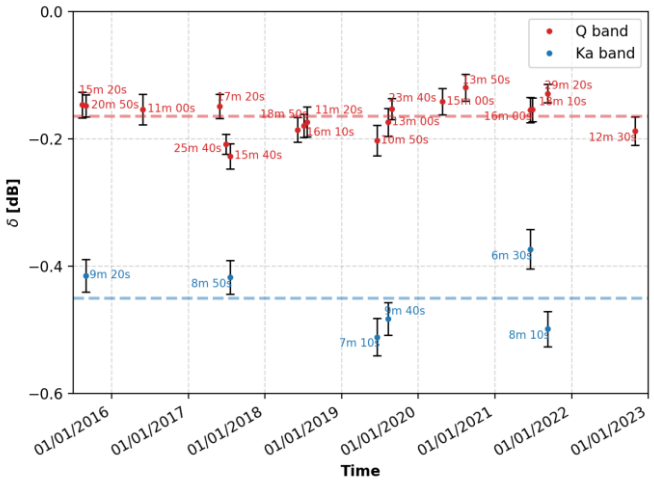

Fig. 15. Values of δ for a few deep fade rain events at Ka (blue) and Q (red) bands, with theoretical one-standard error bars considering white and Gaussian thermal noise. The dashed lines are the weighted average of the values δ_i at Ka (blue) and Q (red) bands.

Nevertheless, the noise power spectral density estimator can now be modified to mitigate the slight difference in gain between the beacon frequency band and the adjacent frequency band:

$$\widehat{N_0}' \overset{\text{def}}{=} \delta \cdot \widehat{N_0}. \tag{53}$$

During deep fades, the signal can be considered as absent, i.e. $P = 0$. From (13) and (27), it follows that the PDF of the ratio R of S to N, normalized to their bandwidth, only depends on known parameters:

$$R \overset{\text{def}}{=} \frac{S}{N} \cdot \frac{B_N}{B_S} \sim \frac{m}{n} \cdot \frac{\chi^2(2n)}{\chi^2(2m)}. \tag{54}$$

The PDF of R is known as a non-central F distribution with $2n$ and $2m$ degrees of freedom [29]:

$$R \sim F_{2n,2m}. \tag{55}$$

Because m is much greater than n, the $F_{2n,2m}$ distribution is almost indiscernible from a $\chi^2(2n)/2n$ distribution.

The empirical PDFs of the samples R collected during the deep fade events identified on Fig. 15 are shown on Fig. 16 at (a) Ka-band and (b) Q-band, along with their theoretical distribution in red dashed curves, under the hypothesis of a white Gaussian noise, as well as the $F_{2n,2m}$ distribution using a correction factor δ. The theoretical histogram is a good fit for the experimental data, indicating that the noise generated by the sky and by the receiver is indeed Gaussian.

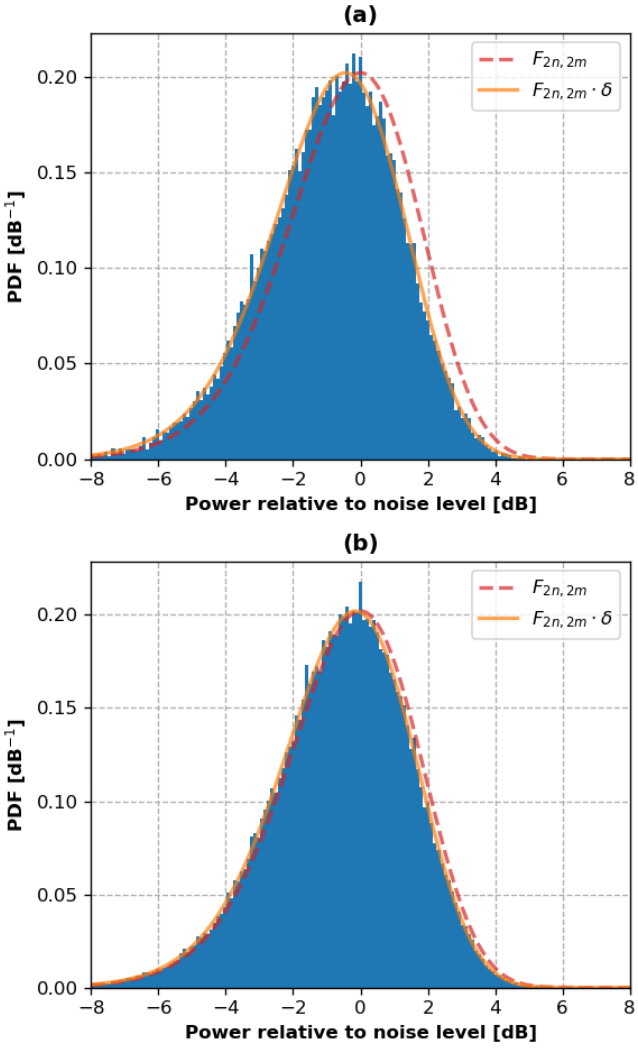

Fig. 16. Empirical PDFs of the samples R during deep fade events at Ka-band (a) and at Q-band (b), along with the theoretical $F_{n,m}$ distribution in red, and the distribution corrected by a factor δ in orange.

The time series of excess attenuation are then computed from the power level S_{dBW}^{filt}, using each of the three estimators defined in this paper. A rain event example is shown in Fig. 17, with the time series of attenuation at Ka-band (blue), and at Q-band (red). The attenuation saturates at Q-band, but not

at Ka-band, due to the higher EIRP of the satellite. The customary estimator $\widehat{P_{dBW}^{filt}}^{(1)}$ is displayed as dashed lines, whereas the new logarithmic estimator $\widehat{P_{dBW}^{filt}}^{(3)}$ is in plain lines. At Ka-band, the difference between the two estimators reaches 5 dB at the peak attenuation. At Q-band, the receiver saturates between 14:46 and 15:01, so the estimated attenuation is accurate for none of the estimators. For the logarithmic estimator $\widehat{P_{dBW}^{filt}}^{(3)}$, data exceeding the dynamic range have been displayed with dotted lines. The value of the dynamic range has been set using Fig. 11: if the maximum acceptable RMSE ($\Delta^{(2)}$) is 1 dB, the dynamic range is reached for a C/N_0 of 10 dB, corresponding for this receiver to 40 dB of attenuation (considering a 50 Hz bandwidth and a clear-sky SNR close to 32 dB). Ideally, the dynamic range should be set by characterizing the receiver in a laboratory, by checking that the output of the beacon receiver corresponds to a controlled input value. It is interesting to note that between 14:55 and 15:00, although the proposed estimator is beyond its dynamic range, the estimated attenuation is lower than the attenuation between 14:41 and 14:55. This is consistent with the attenuation at Ka band, which is lower at the same time frame. While the error is probably too high for most applications, this indicates that the beacon frequency band is still aligned with the carrier frequency, even at very low signal-to-noise ratios.

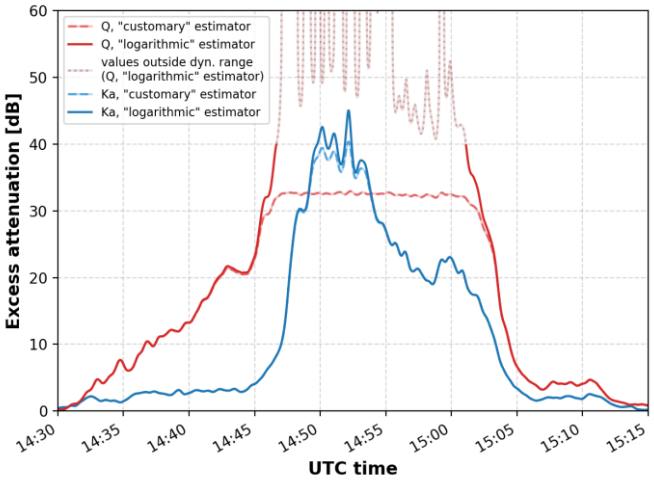

Fig. 17. Rain event measured on the 12th of August, 2020, in Toulouse, at Ka and Q bands.

Now, 7 years of propagation measurements collected at Ka and Q bands in Toulouse are used to compute reliable CCDFs of excess attenuation at both frequencies (see Fig. 18). Due to the absence of a 'true' value of the attenuation, the dynamic range of each estimator has been set using simulated results (see Fig. 12): in the case of CCDFs, the dynamic range is defined as the highest value of attenuation, for which the difference between the estimated CCDF and the true CCDF is lower than 0.5 dB (analogous to the definition in (9) for time series). This corresponds, for the customary, natural and logarithmic estimators, to respectively 24 dB, 32 dB and 42 dB at Q-band, and to 33 dB, 41 dB and 51 dB at Ka band.

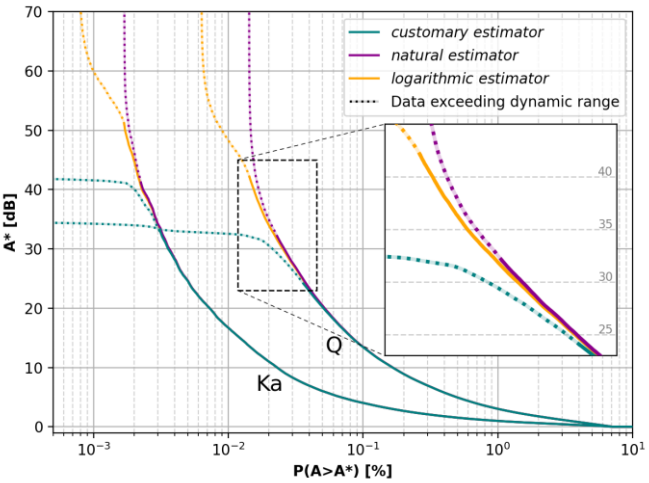

Fig. 18. CCDFs of rain attenuation at Ka and Q band, measured in Toulouse between 2016 and 2022 (7 years), using the three different estimators.

VIII. Conclusion

In this paper a methodology is described to increase the dynamic range of propagation measurements carried out from satellite beacon signals. This is possible because the noise power is measured in a wide frequency band adjacent to the beacon frequency (typically several tens of kHz), in addition to the usual measurements of the beacon power in a narrow frequency band around the beacon frequency (typically several tens of Hz).

Three estimators of the power received from a satellite beacon, respectively referred as the customary, natural, and logarithmic estimators, have been reviewed. The customary estimator $\widehat{P_{dBW}^{filt}}^{(1)}$ directly considers the noisy power measurement to be equal to the beacon signal power. In addition to the measurement of the power in the frequency band of the beacon, the natural $\widehat{P_{dBW}^{filt}}^{(2)}$ and logarithmic $\widehat{P_{dBW}^{filt}}^{(3)}$ estimators require a measurement of the noise power spectral density in an adjacent frequency band. Using simulations under realistic conditions, both estimators result in an extended dynamic range with respect to the customary estimator. The logarithmic estimator is especially accurate to determine high values of attenuation (equivalent to a low signal-to-noise ratio), due to its processing in decibels.

It remains to be confirmed whether the dynamic range improvements obtained from synthetic data can be transposed to experimental data. Indeed, several assumptions about the receiver have been made to mathematically derive the estimators. Namely, it is assumed that all sources of noise are white and Gaussian, and that the beacon carrier frequency is perfectly estimated. For this reason, the performance of the estimators should be assessed on beacon receivers under laboratory conditions, expressly with a controlled and known input.

Appendix A: Step-by-step Procedure to Compute Corrected Beacon Power

A. *Implementation of the functions h_n*

Following its definition in (45), h_n is expressed from the reciprocal function g_n^{-1} of g_n defined in (35). g_n^{-1} is calculated numerically by interpolating an list of couples

$\big(x, g_n(x)\big)$. For small values of x, and large values of n, the numerical implementation of $g_n(x)$ in (45) produces large errors when using floating-point numerical variables with conventional precision. Therefore, the bounds of the function g_n proposed in [22] are used to mitigate these numerical errors.

Case 1: $n \leq 100$:

1) Generate a vector $(y_i)_{i\in 1..1001}$ geometrically spaced between $0.01 \cdot n$ and $100 \cdot n$, i.e.:

$$\begin{cases} y_0 = 0 \\ for\ 1 \leq i \leq 1001, \quad y_i = 10^{(i-1)/250} \cdot n \end{cases} \tag{A.1}$$

2) Generate a vector $(z_i)_{i\in 1..1001}$, defined as:

$$z_i = \begin{cases} g_n(y_i), & if\ i > 0 \\ \psi(n), & if\ i = 0 \end{cases}, \tag{A.2}$$

where:

$$g_n(y_i) = \ln(y_i) - Ei(-y_i) + \sum_{j=1}^{n-1} \left(-\frac{1}{y_i}\right)^j \cdot \left(e^{-y_i} \cdot (j-1)! - \frac{(n-1)!}{j \cdot (n-1-j)!}\right), \tag{A.3}$$

with $Ei(\cdot)$ the exponential integral function, and $\psi(\cdot)$ the digamma function.

3) Generate a vector $(x_i)_{i\in 1..1001}$, defined as:

$$x_i = \begin{cases} b_l & if\ z_i < b_l \\ z_i & if\ b_l \leq z_i \leq b_u \\ b_u & if\ b_u < z_i \end{cases}, \tag{A.4}$$

where:

$$b_l = \ln\left(\frac{z_i + n}{n}\right) + \psi(n), \tag{A.5}$$

and

$$b_u = \frac{n+1}{n} \cdot \ln\left(\frac{z_i + n + 1}{n+1}\right) + \psi(n). \tag{A.6}$$

4) Numerical interpolation to define g_n^{-1}:

$g_n^{-1}(x)$ is defined solely if $x \geq x_0$, with $x_0 = \psi(n)$.

- If $x_0 \leq x \leq x_n$, $g_n^{-1}(x)$ is defined as the linear interpolation of the points (x_i, y_i) at the point x.
- If $x_n < x$, $g_n^{-1}(x)$ is defined as

$$g_n^{-1}(x) = e^x - n + 1. \tag{A.7}$$

5) Finally, the function h_n is defined for all $u \geq 0$ as

$$h_n(u) = \begin{cases} 10\log_{10}\left(\frac{1}{n \cdot u} \cdot g_n^{-1}(\ln(n \cdot u))\right) & if\ u > \frac{e^{\psi(n)}}{n} \\ -\infty & else \end{cases} \tag{A.8}$$

Case 2: $n > 100$:

In this case, the function h_n is simply defined for all $u \geq 0$ as

$$h_n(u) = 10 \cdot \log_{10}\left(1 - \frac{1}{u}\right). \tag{A.9}$$

B. Step-by-step procedure

It is assumed that a receiver delivers the samples $S(k \cdot T_I)$ and $N(k \cdot T_I)$, in watts, respectively measured in the frequency bands of the beacon (with a narrow bandwidth B_S) and in an adjacent frequency band where solely the thermal noise is present (with a wider bandwidth B_N), with a sampling period of T_I in seconds. One should be careful that, in the following equations, $N(k \cdot T_I)$ is not normalized by B_S/B_N as it is sometimes the case.

Let S_{dBW} be the logarithm of the power in dBW:

$$S_{dBW}(k \cdot T_I) \overset{\text{def}}{=} 10\log_{10}\big(S(k \cdot T_I)\big), \tag{A.10}$$

and

$$n = B_S \cdot T_I. \tag{A.11}$$

It will be assumed that n is an integer.

The step-by-step methodology described hereafter can be followed:

1) Compute the noise power spectral density N_0 (in W/Hz) using the following formula:

$$\widehat{N_0}(k \cdot T_I) = \frac{1}{(2l+1) \cdot B_N} \sum_{i=-l}^{l} N\big((k+i) \cdot T_I\big), \tag{A.12}$$

with:

$$l = \left\lfloor \frac{5}{T_I} \right\rfloor, \tag{A.13}$$

where $\lfloor \cdot \rfloor$ is the floor function ($(A.13)$ corresponds to an integration time of 10 seconds).

2) Low-pass filter the signal:

$$S_{dBW}^{filt}(k \cdot T_I) = (\hbar \star S_{dB})(k \cdot T_I), \tag{A.14}$$

where $\hbar$ is the impulse response of the low-pass filter, and $\star$ is the convolution operation (the cut-off frequency of the filter is usually set to 0.025 Hz in temperate climates). Note that for applications requiring synchronicity, zero-phase filters are usually used (such as forward-backward filters).

3) Compute the samples of estimated power level $\widehat{P_{dBW}^{filt}}^{(3)}(k \cdot T_I)$:

$$\widehat{P_{dBW}^{filt}}^{(3)}(k \cdot T_I) = S_{dBW}^{filt}(k \cdot T_I) + h_n\left(\frac{10^{\left(\frac{S_{dBW}^{filt}(k \cdot T_I)}{10}\right)}}{B_S \cdot \widehat{N_0}}\right) \tag{A.15}$$

The samples $\widehat{P_{dBW}^{filt}}^{(3)}(k \cdot T_I)$, expressed in dBW, can then be used as in the conventional procedure to compute attenuation in (2), i.e. by removing the reference power level set by the experimenter (which is equal to the clear sky level if the goal is to obtain excess attenuation).

APPENDIX B: PROOF THAT THE LOGARITHMIC ESTIMATOR ASYMPTOTICALLY CONVERGES TO THE NATURAL ESTIMATOR AS N TENDS TO INFINITY

From the definitions of the logarithmic estimator in (44) and the natural estimator in (42), it is equivalent to show that h_n, defined in (45), asymptotically converges to h, defined in (43), as n tends to infinity. From [22], Theorem 7, for $z \geq 0$, and $n \geq 1$, we have:

$$\ln(z+n-1) \leq g_n(z) \leq \ln(z+n). \quad (B.1)$$

From [22], Proposition 6, g_n is a strictly increasing function. Therefore, its inverse, g_n^{-1} is also strictly increasing. Consequently:

$$g_n^{-1}(\ln(z+n-1)) \leq g_n^{-1}\big(g_n(z)\big) \leq g_n^{-1}(\ln(z+n)), \quad (B.2)$$

so

$$g_n^{-1}(\ln(z+n-1)) \leq z \leq g_n^{-1}(\ln(z+n)), \quad (B.3)$$

which can be rewritten as

$$\begin{cases} g_n^{-1}(\ln(z+n-1)) \leq e^{\ln(z+n-1)} - n + 1 \\ e^{\ln(z+n)} - n \leq g_n^{-1}(\ln(z+n)) \end{cases}. \quad (B.4)$$

Let $u = \ln(z+n-1)$, and $v = \ln(z+n)$. Equation (B.4) becomes

$$\begin{cases} g_n^{-1}(u) \leq e^u - n + 1 \\ e^v - n \leq g_n^{-1}(v) \end{cases}, \quad (B.5)$$

or, equivalently,

$$e^y - n \leq g_n^{-1}(y) \leq e^y - n + 1. \quad (B.6)$$

Let $x = \frac{e^y}{n}$, then

$$n \cdot x - n \leq g_n^{-1}(\ln(n \cdot x)) \leq n \cdot x - n + 1. \quad (B.7)$$

Case 1: $x > 1$:

Equation (B.7) can be rewritten

$$1 - \frac{1}{x} \leq \frac{g_n^{-1}(\ln(n \cdot x))}{n \cdot x} \leq 1 - \frac{1}{x} + \frac{1}{n \cdot x}. \quad (B.8)$$

Because the logarithm is a strictly increasing function,

$$10 \cdot \log_{10}\left(1 - \frac{1}{x}\right) \leq 10 \cdot \log_{10}\left(\frac{g_n^{-1}(\ln(n \cdot x))}{n \cdot x}\right) \leq 10 \cdot \log_{10}\left(1 - \frac{1}{x} + \frac{1}{n \cdot x}\right). \quad (B.9)$$

Because:

$$\lim_{n\to\infty} 10 \cdot \log_{10}\left(1 - \frac{1}{x} + \frac{1}{n \cdot x}\right) = 10 \cdot \log_{10}\left(1 - \frac{1}{x}\right), \quad (B.10)$$

using the squeeze theorem, we get:

$$\lim_{n\to\infty} 10 \cdot \log_{10}\left(\frac{g_n^{-1}(\ln(n \cdot x))}{n \cdot x}\right) = 10 \cdot \log_{10}\left(1 - \frac{1}{x}\right). \quad (B.11)$$

$$\lim_{n\to\infty} h_n(x) = 10 \cdot \log_{10}\left(1 - \frac{1}{x}\right) = h(x) \quad (B.12)$$

Case 2: $0 < x \leq 1$:

By definition, the natural estimator gives $-\infty$.

$$\lim_{n\to\infty} \frac{e^{\psi(n)}}{n} = 0 \quad (B.13)$$

Because x is strictly positive, after a certain rank n_0, $\frac{e^{\psi(n)}}{n} < x$.

Using the definition of h_n, for $n \geq n_0$, $h_n(x) = -\infty$. Therefore,

$$\lim_{n\to\infty} h_n(x) = -\infty = h(x) \quad (B.14)$$

Case 2: $x = 0$:

By definition, h and h_n both equal $-\infty$.

APPENDIX C: PROOF THAT THE RMSE OF THE LOGARITHMIC ESTIMATOR IS A SOLE FUNCTION OF THE SIGNAL-TO-NOISE RATIO

Under stationarity conditions, two parameters affect the Root Mean Square Error (RMSE) of the logarithmic estimator: P and σ_S. Indeed, its definition is as follows:

$$RMSE \overset{\text{def}}{=} \sqrt{\mathbb{E}\left[\left(\widehat{P_{dBW}} - P_{dBW}\right)^2\right]}, \quad (C.1)$$

where $\widehat{P_{dBW}}$ is the logarithmic estimator defined as

$$\widehat{P_{dBW}} \overset{\text{def}}{=} 10\log_{10}(S) + h_n\left(\frac{S}{B_S \cdot \widehat{N_0}}\right), \quad (C.2)$$

with h_n the function defined in (45).

In fact, the quantity

$$\widehat{P_{dBW}} - P_{dBW} = 10\log_{10}\left(\frac{S}{P}\right) + h_n\left(\frac{S}{B_S \cdot \widehat{N_0}}\right) \quad (C.3)$$

can be expressed a function of a single parameter, the signal-to-noise ratio ξ (SNR in the body of the paper), with the following definition:

$$\xi \overset{\text{def}}{=} \frac{P}{\sigma_S^2}. \quad (C.4)$$

Using (27),

$$\frac{S}{P} \sim \frac{\sigma_S^2}{2n \cdot P} \cdot \chi_{nc}^2\left(2n; \frac{2n \cdot P}{\sigma_S^2}\right), \quad (C.5)$$

where the symbol $\sim$ denotes the equality in distribution. Equivalently,

$$\frac{S}{P} \sim \frac{1}{2n \cdot \xi} \cdot \chi_{nc}^2(2n; 2n \cdot \xi), \quad (C.6)$$

which shows that the first member of $(C.3)$ only depends on the signal-to-noise ratio.

From (13) and (19), considering that N is a stationary process,

$$\widehat{N_0} \sim \frac{\sigma_N^2}{2m \cdot l \cdot B_N} \cdot \chi^2(2m \cdot l). \quad (C.7)$$

Using (17) and (31), it follows that

$$\frac{S}{B_S \cdot \widehat{N_0}} \sim \frac{\frac{\sigma_S^2}{2n} \cdot \chi_{nc}^2\left(2n; \frac{2n \cdot P}{\sigma^2}\right)}{\frac{\sigma_S^2}{2m} \cdot \chi^2(2m)}, \quad (C.8)$$

or equivalently,

$$\frac{S}{B_S \cdot \widehat{N_0}} \sim \frac{m \cdot \chi_{nc}^2(2n; 2n \cdot \xi)}{n \cdot \chi^2(2m)}, \quad (C.9)$$

therefore the second member of $(C.3)$ also depends solely on the signal-to-noise ratio ξ. Consequently, the root mean square error of the logarithmic estimator defined in $(C.1)$ only depends on the signal-to-noise ratio.

ACKNOWLEDGMENT

The authors would like to thank Prof. Michel Bousquet and Dr. Arsim Kelmendi for their critical review and relevant suggestions.

REFERENCES

[1] J. P. Baptista and G. Davies, 'OPEX, Volume 1: Reference Book on Attenuation Measurement and Prediction', in *Second Workshop of the OLYMPUS Propagation Experimenters*, Noordwijk, Nov. 1994.

[2] J. Belshaw, 'Reference Book on Data Processing', in *Second Workshop of the OLYMPUS Propagation Experimenters*, Noordwijk, Nov. 1994.

[3] L. Castanet, M. Bousquet, and D. Mertens, ‘Simulation of the performance of a Ka-band VSAT videoconferencing system with uplink power control and data rate reduction to mitigate atmospheric propagation effects’, *Int. J. Satell. Commun.*, vol. 20, no. 4, pp. 231–249, Jul. 2002, doi: 10.1002/sat.722.

[4] C. J. Kikkert and O. P. Kenny, ‘A digital signal processing based Ka band Satellite Beacon Receiver / Radiometer’, in *2008 2nd International Conference on Signal Processing and Communication Systems*, Gold Coast, Australia: IEEE, Dec. 2008, pp. 1–8. doi: 10.1109/ICSPCS.2008.4813688.

[5] F. Machado, E. Vilar, F. P. Fontán, V. Pastoriza, and P. Mariño, ‘Easy-to-Build Satellite Beacon Receiver for Propagation Experimentation at Millimeter Bands’, *Radioengineering*, vol. 23, no. 1, 2014.

[6] J. Nessel, J. Morse, M. Zemba, C. Riva, and L. Luini, ‘Performance of the NASA beacon receiver for the Alphasat Aldo Paraboni TDP5 propagation experiment’, in *2015 IEEE Aerospace Conference*, Big Sky, MT: IEEE, Mar. 2015, pp. 1–8. doi: 10.1109/AERO.2015.7119311.

[7] A. Hrovat, G. Kandus, U. Kuhar, A. Kelmendi, and A. Vilhar, ‘A Ka-band Satellite Beacon Receiver for Propagation Experiment’, *Journal of Microelectronics, Electronic Components and Materials*, vol. 46, no. 1, 2016.

[8] V. Pastoriza-Santos, F. Machado, D. Nandi, and F. Pérez-Fontán, ‘Low-Cost Ka-Band Satellite Receiver Data Preprocessing for Tropospheric Propagation Studies’, *Sensors*, vol. 22, no. 3, p. 1043, Jan. 2022, doi: 10.3390/s22031043.

[9] C. J. Kikkert, ‘Dynamic Range Improvements of a Beacon Receiver Using DSP Techniques’, *Proceedings of URSI Commission F Triennium Open Symposium 2004*.

[10] A. Costouri, J. Nessel, and G. Goussetis, ‘Validation of a Digital Noise Power Integration Technique for Radiometric Clear Sky Attenuation Estimation at Q-Band’, *IEEE Trans. Antennas Propagat.*, vol. 68, no. 9, pp. 6743–6751, Sep. 2020, doi: 10.1109/TAP.2020.3001452.

[11] F. J. Harris, ‘On the use of windows for harmonic analysis with the discrete Fourier transform’, *Proc. IEEE*, vol. 66, no. 1, pp. 51–83, 1978, doi: 10.1109/PROC.1978.10837.

[12] M. Schwartz, W. R. Bennett, and S. Stein, *Communication systems and techniques*, IEEE Press ed. New York: IEEE Press, 2010.

[13] X. Boulanger, B. Gabard, L. Casadebaig, and L. Castanet, ‘Four Years of Total Attenuation Statistics of Earth-Space Propagation Experiments at Ka-Band in Toulouse’, *IEEE Trans. Antennas Propagat.*, vol. 63, no. 5, pp. 2203–2214, May 2015, doi: 10.1109/TAP.2015.2407376.

[14] L. Castanet, Ed., *Influence of the variability of the propagation channel on mobile, fixed multimedia and optical satellite communications*. in Berichte aus der Informationstechnik. Aachen: Shaker, 2008.

[15] T. Moulsley and E. Vilar, ‘Experimental and theoretical statistics of microwave amplitude scintillations on satellite down-links’, *IEEE Trans. Antennas Propagat.*, vol. 30, no. 6, pp. 1099–1106, Nov. 1982, doi: 10.1109/TAP.1982.1142964.

[16] L. Luini, G. A. Siles, J. M. Riera, C. G. Riva, and J. Nessel, ‘Methods to Estimate Gas Attenuation in Absence of a Radiometer to Support Satellite Propagation Experiments’, *IEEE Trans. Instrum. Meas.*, vol. 69, no. 7, pp. 5116–5127, Jul. 2020, doi: 10.1109/TIM.2019.2950612.

[17] U. L. Rohde and J. C. Whitaker, *Communications receivers: DSP, software radios, and design*, 3rd ed. New York: McGraw-Hill, 2001.

[18] C. Drentea, *Modern communications receiver design and technology*. in Artech House intelligence and information operations series. Boston, Mass: Artech House, 2010.

[19] U. Grenander, H. O. Pollak, and D. Slepian, ‘The Distribution of Quadratic Forms in Normal Variates: A Small Sample Theory with Applications to Spectral Analysis’, *Journal of the Society for Industrial and Applied Mathematics*, vol. 7, no. 4, pp. 374–401, Dec. 1959, doi: 10.1137/0107032.

[20] C. Walck, ‘Hand-book on Statistical Distributions for Experimentalists’. Sep. 10, 2007.

[21] H. Urkowitz, ‘Energy detection of unknown deterministic signals’, *Proc. IEEE*, vol. 55, no. 4, pp. 523–531, 1967, doi: 10.1109/PROC.1967.5573.

[22] S. Moser, ‘Expected Logarithm and Negative Integer Moments of a Noncentral $\chi 2$-Distributed Random Variable’, *Entropy*, vol. 22, no. 9, p. 1048, Sep. 2020, doi: 10.3390/e22091048.

[23] ‘Recommendation ITU-R P.1853-2: Time series synthesis of tropospheric impairments’, p. 31, Aug. 2019.

[24] G. Maral, M. Bousquet, and Z. Sun, ‘System Noise Temperature’, in *Satellite communications systems: systems, techniques and technology*, Sixth edition., Hoboken, N.J: John Wiley & Sons, 2020, pp. 211–213.

[25] ‘Recommendation ITU-R P.372-16: Radio Noise’. Aug. 2022.

[26] P. C. F. Eggers, I. Syrytsin, and J. Kristmundsson, ‘A low cost Dual-branch Q-band 39.4 GHz I/Q Satellite Beacon Receiver for Atmospheric Propagation Studies’, in *2022 16th European Conference on Antennas and Propagation (EuCAP)*, Madrid, Spain: IEEE, Mar. 2022, pp. 1–5. doi: 10.23919/EuCAP53622.2022.9769544.

[27] M. J. Zemba, J. R. Morse, and J. A. Nessel, ‘Frequency estimator performance for a software-based beacon receiver’, in *2014 IEEE Antennas and Propagation Society International Symposium (APSURSI)*, Memphis, TN, USA: IEEE, Jul. 2014, pp. 1574–1575. doi: 10.1109/APS.2014.6905113.

[28] X. Boulanger and L. Castanet, ‘Ka and Q band propagation experiments in Toulouse using ASTRA 3B and ALPHASAT satellites’, *Int J Satell Commun Network*, vol. 37, no. 5, pp. 449–459, Sep. 2019, doi: 10.1002/sat.1261.

[29] N. L. Johnson, S. Kotz, and N. Balakrishnan, *Continuous univariate distributions volume 2*, 2nd ed. in Wiley series in probability and mathematical statistics. New York: Wiley, 1994.